Journal of Applied Polymer Science

Morphology and Mechanical Properties of Heterophasic PP-EP/EVA/Organoclay Nanocomposites

Adriana Berenice Espinoza-Martínez,[1] Eduardo Ramírez-Vargas,[1] Saúl Sánchez-Valdes,[1] Luis Francisco Ramos de Valle,[1] Francisco J. Medellín-Rodríguez,[2] Benjamin S. Hsiao,[3] Lixia Rong,[3] Mario Valera Zaragoza[4]

[1]Departamento de Procesado, Centro de Investigación en Química Aplicada, Saltillo, Coahuila 25294, México
[2]CIEP-FCQ, UASLP, Zona Universitaria, San Luis Potosí 78210, México
[3]Department of Chemistry, State University of New York at Stony Brook, Stony Brook, New York 11794-3400
[4]Departamento de Materiales, Universidad del Papaloapan, Circuito Central 200, Parque Industrial Tuxtepec, Oaxaca 68301, México
Correspondence to: E. Ramírez-Vargas (E-mail: evargas@ciqa.mx)

ABSTRACT: The effect of vinyl acetat (VA) on the morphological, thermal stability, and mechanical properties of heterophasic polypropylene–(ethylene-propylene) copolymer (PP–EP)/poly(ethylene vinyl acetate) (EVA)/organoclay nanocomposites was studied. Tailored organoclay C20A was selected to enhance the exfoliation of the clay platelets. Depending on the VA content, there were two morphological organoclay populations in the systems. Both populations were directly observed by scanning transmission electron microscopy and measured by wide-angle X-ray diffraction and small-angle X-ray scattering. The content of VA in EVA originated spherical and elongated morphologies in the resultant nanocomposites. High-VA content led to a better intercalation of the organoclay platelets. Measurement of thermal properties suggested that higher VA decreases thermal stability in samples both with and without organoclay, although nanocomposites had higher thermal stability than samples without clay. The storage modulus increased both with nanoclay and VA content. © 2012 Wiley Periodicals, Inc. J. Appl. Polym. Sci. 000: 000–000, 2012

KEYWORDS: nanocomposites; organoclay; PP–EP/EVA; morphology

Received 26 April 2012; accepted 4 September 2012; published online
DOI: 10.1002/app.38553

INTRODUCTION

Polymer–clay nanocomposites are a new class of materials that often display better physical, chemical, and mechanical properties than their neat polymers[1–4]; therefore, they have attracted attention for novel industrial applications. Nevertheless, the main technical challenge to commercialize the emerging products is to have good dispersion and exfoliation of the nanoclay component. These two characteristics will enhance the positive effect of the clay platelets on the properties of the polymeric nanocomposite.[5–7] The exfoliated condition can be easily achieved for specific polar polymers; however, in the case of nonpolar polymeric systems, such as polypropylene–(ethylene-propylene) (PP–EP) copolymers, a second component, that is, poly(ethyl vinyl acetate) (EVA), can help both to host and exfoliate the nanoclay. It is known[8] that ion-exchanged nanoclays can help the process of macromolecular intercalation within the nanoclay galleries. It has been reported, for example, that the molecular characteristics of ion-exchanged surfactants, such as the number and length of substitute molecules, can help the exfoliation of clay nanolayers.[9,10] In other cases, in which polar molecules are included, such as maleic anhydride, enhanced compatibility between polymer and nanoclay can be attained, as in the case of polyethylene[11] and polypropylene[12] functionalized with maleic anhydride. Wang et al.[13] determined, for example, that the content of maleic anhydride in polyethylene mixtures plays an important role in nanoclay exfoliation. In addition, polarity of the ester group in rubbery EVA has also been used to obtain intercalated systems without the need of compatibilizers.[14,15] It has been reported that EVA interacts with the exchanged molecules on the nanoclay surface[16] and that the generation of exfoliated clay in EVA depends not only on the EVA type but also on the vinyl acetate (VA) content and processing conditions. In a previous study,[17] with PP–EP/EVA/organoclay systems, a range of compatibility between PP–EP and EVA was determined, and also a change in morphology depending on EVA concentration was observed. Clay exfoliation within the EVA component increased thermal stability of the polymeric system.[18] Because VA in EVA is very important in ternary (PP–EP/EVA/organoclay) polymeric nanocomposites,

the main objective of the present study is to fulfill this gap. EVA copolymers with different VA contents and similar flow properties are selected. Morphology, thermal stability, and mechanical properties are discussed.

EXPERIMENTAL

Materials

Heterophasic PP–EP copolymer, with a melt flow index (MFI) of 4 g/10 min, was from Montell Polyolefins, USA, with 8 wt % of ethylene content and a density of 0.9 g/cm^3. EVA copolymers were from Dupont, USA, having 9, 18, and 28 wt % VA with MFI of 7, 8, and 6 g/10 min, respectively. Organoclay Cloisite 20 A® with dimethyl di(hydrogenated tallow alkyl) ammonium cations was a commercial product from Southern Clay, USA, with 38.7 wt % surfactant content and an interlayer spacing of 2.5 nm.

Nanocomposites Preparation

PP–EP/EVA/organoclay nanocomposites were prepared by melt compounding in a corotating twin screw extruder. The screw configuration used was medium shear, as reported elsewhere.[17] Both organoclay and polymer pellets were dried at 60°C for at least 3 h before any processing, and the nanocomposites were obtained in two steps. In the first step, mixtures of EVA pellets and organoclay (86/14 wt %/wt %) were melt-mixed at 130°C and a screw rate of 100 rpm. Then, in a second step, the EVA/organoclay mixture and the PP–EP heterophasic copolymer (56/44 wt %) were melt-mixed at 190°C and 100 rpm. Thereafter, pellets of PP–EP/EVA/organoclay nanocomposites were injection-molded in order to obtain samples for further characterization. The injection molding was carried out at 220°C with injection pressure of 3.8 MPa.

Characterization

Wide-Angle X-Ray Diffraction. X-ray diffraction patterns were obtained in a Siemens D-5000 X-ray diffractometer, using a Ni-filtered Cu Kα radiation generator. The diffraction patterns were collected in the 2θ range 1°–10° with a scanning rate of 0.4°/min, 25 mA for the intensity of the filament, and an accelerating voltage of 35 kV. Bragg's law, $d = n\lambda/2 \sin \theta$, was used to estimate the corresponding clay interlayer spacing of the different nanocomposites where n is an integer, λ is the wavelength of the incident wave, d is the spacing between the planes in the atomic lattice, and θ is the angle between the incident ray and the scattering planes.

Small Angle X-Ray Scattering. The periodic structure of silicate layers in PP–EP/EVA/organoclay nanocomposites was determined by synchrotron small-angle X-ray scattering (SAXS) at the X27C beamline in the National Synchrotron Light Source in Brookheaven National Laboratory, USA. The diffracting angle was calibrated by the Ag-Be standard. Samples were placed in perpendicular position regarding the X-ray beam, and all experiments were carried out at room temperature. The collected images were processed in the POLAR software (Stony Brook Technology and Applied Research). SAXS data were corrected using the Lorentz's factor before calculating the samples' periodicity via $L = 2\pi/q_{max}$, where L is the average lamellar thickness and q_{max} is the scattering vector value at the peak (nm^{-1}).

Scanning Electron Microscopy. To study the dispersion of EVA in the PP–EP matrix, the surface of cryogenically fractured injection-molded samples was etched with toluene at 40°C for 2 h to remove the EVA phase and then observed using a Topcon sm.510 scanning electron microscope. Before imaging, samples were sputter-coated with a mixture of Au-Pd. The SEM micrographs were taken at an accelerating voltage of 15 kV.

Scanning Transmission Electron Microscopy. Exfoliation analyses of clay nanolayers were carried out in a JOEL JSM-7401 field-emission scanning electron microscope with scanning transmission electron microscopy (STEM) and secondary electron detectors and an acceleration voltage of 25 and 30 kV. Ultrathin sections of samples were previously obtained through the use of an ultramicrotome equipped with a diamond knife.

Thermogravimetric Analyses. Thermogravimetric analyses of the PP–EP/EVA blends and nanocomposites were carried out in a DuPont Instruments 951 Thermogravimetrical Analyzer. A heating rate of 20°C/min was used along the whole temperature range from 25 to 600°C using nitrogen atmosphere and from 600 to 800°C using air atmosphere.

Dynamic Mechanical Analysis. Dynamic mechanical analysis (DMA) was used to determine viscoelastic properties of the studied nanocomposites as a function of temperature. Samples were analyzed on a TA Instruments Dynamic Mechanical Analyzer (DMA 938).The clamp model was a double cantilever, and the experimental conditions included a frequency of 0.1 Hz, oscillation amplitude from 0.3 to 0.5 mm, and heating rate of 5°C/min from −80 to 80°C.

RESULTS AND DISCUSSION

Structure of Nanocomposites

Three component polymeric systems are often considered complex, because, depending on preparation conditions, the resultant morphology involves several possibilities. Therefore, morphological characterization of the resultant products has to be systematically made. This is the case of PP–EP/EVA/organoclay nanocomposites, where a heterophasic copolymer, a rubbery phase, and an inorganic additive are the constitutive components. Figure 1 shows X-ray diffraction results of PP–EP/EVAx blends samples and PP–EP/EVAx/organoclay nanocomposites samples (x = wt % VA content), where the lack of diffracting reflections at lower angles for the reference samples can be observed. However, Cloisite 20A shows a characteristic d_{001} diffraction peak located around 3.7° corresponding to a basal interlayer spacing of 2.5 nm[19] according to Bragg's equation. The d_{001} peak of the clay is well defined for the nanocomposites, suggesting that a complete exfoliation of the platelets did not occur. However, this peak is shifted to lower angles, suggesting that intercalated–exfoliated structure was obtained, as reported for La Mantia et al.[20] for EVA organoclay nanocomposites. This double reflection effect suggests that at least two nanoclay populations, with different periodicities, are present in the studied nanocomposites. The two peaks gradually tend to disappear as the VA content in EVA increases, and the

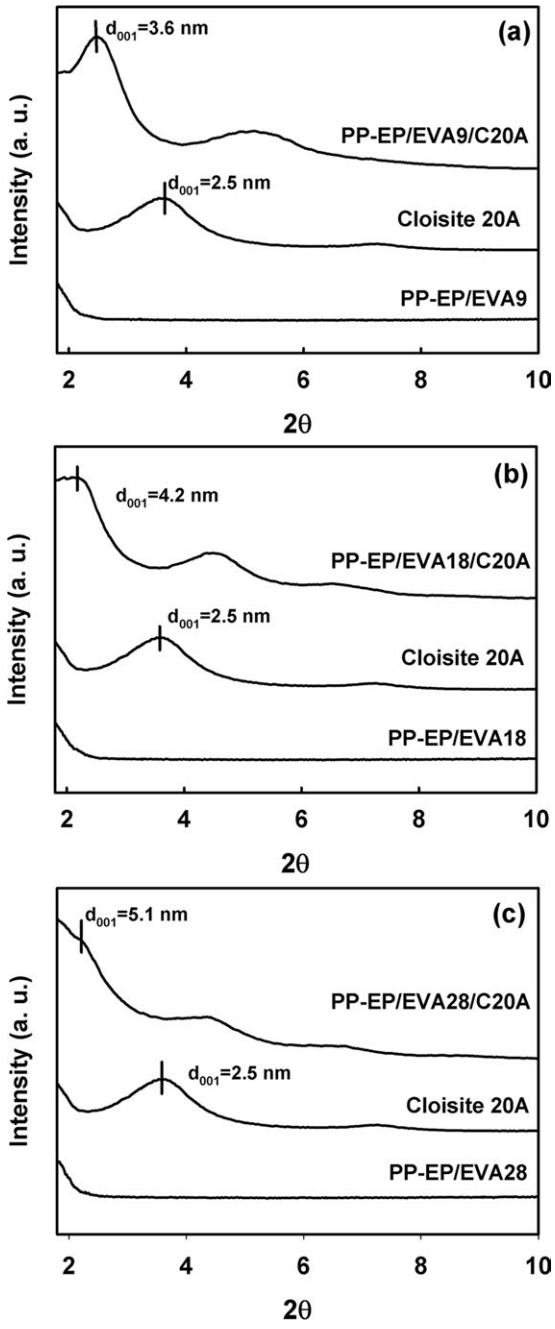

Figure 1. X-ray diffraction patterns of PP–EP/EVAx and PP–EP/EVAx/organoclay nanocomposites with different VA content (a) 9% VA, (b) 18% VA, and (c) 28% VA.

explanation is directly related to the nanostructuration of the nanocomposites. As shown in Figure 1, the interlayer spacing of the organoclay increases from 2.5 to 3.6 nm for the case of PP–EP/EVA9/C20A and to 4.2 and 5.1 nm for PP–EP/EVA18/C20A and PP–EP/EVA28/C20A, respectively. These results clearly show the improved intercalated–exfoliated morphology for these nanocomposites with increasing VA content.

STEM images confirm the presence of two nanoclay populations in most of nanocomposites. One could be linked to the high-periodicity galleries, that is, intercalated–exfoliated nanoclay (population I), and the other could be associated to the so-called tactoids (population II). Figure 2(c) shows the disappearance of population II in PP–EP/EVA28/C20A nanocomposite, that is, in the nanocomposite with higher VA in EVA. At this point, one could expect that the presence of more polar groups in EVA copolymer promotes noncovalent interactions with the clay surface as been reported in literature.[21,22] Thus, it allows the homogeneous intercalation of polymeric chains into the clay galleries. These results are in agreement with those obtained by Pasanovic-Zujo et al.[16] who reported intercalated–exfoliated structures in EVA/

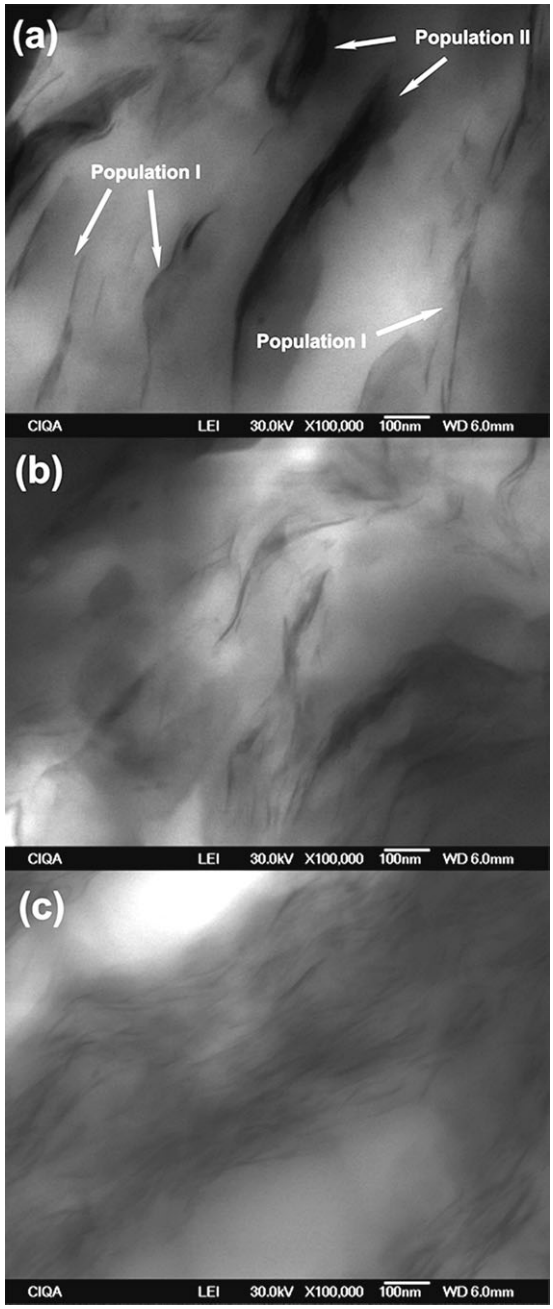

Figure 2. STEM images of PP–EP/EVAx and PP–EP/EVAx/organoclay nanocomposites: (a) PP–EP/EVA9/C20A, (b) PP–EP/EVA18/C20A, and (c) PP–EP/EVA28/C20A.

Applied Polymer SCIENCE

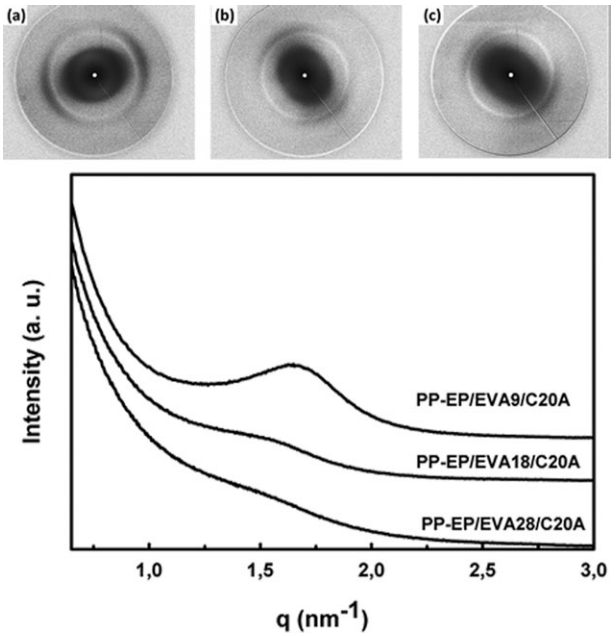

Figure 3. SAXS patterns of PP–EP/EVA/organoclay nanocomposites: (a) PP–EP/EVA9/C20A, (b) PP–EP/EVA18/C20A, and (c) PP–EP/EVA28/C20A.

nanoclay nanocomposites with 18 and 28 wt % VA and intercalated structures with low-VA content (9 wt %).

The SAXS results in Figure 3 allow the identification of scattering maxima with periodicities within the range of population 3.5–4.2 nm as shown in Table I, corresponding to the first diffraction maxima in the wide-angle X-ray diffraction results discussed before (population I). SAXS images show in addition that nanoclays are slightly oriented regarding the sample planar direction. This is most probably due to the processing conditions that were used to generate the experimental probes, although nanoclays have also been considered orientation promoters by themselves.[23] In a previous study concerning PP–EP/EVA, it was proposed that the nanoclay tends to preferentially confined in the EVA phase.[18] This statement was made considering the low-EVA viscosity and the preparation method, which involves, as a first step, mixing of nanoclay and EVA.

Phase Morphology

In previous studies[24,25] of PP–EP/EVA blends with different ratios (different concentration of polar groups), a compatibility range between 80/20 and 60/40 wt % ratio was found. There were found two morphological transitions depending on EVA concentration. The first was observed above 20 wt % EVA and consisted of a change from spherical to elongated domains. The second transition succeeded above 40 wt % EVA, and the change was from elongated to fibroid structures. For this reason, in the present work, a 60/40 wt % PP–EP/EVA ratio was chosen. SEM results (Figure 4) give evidence of phase-morphological changes as a function of VA content in EVA. It is observed that EVA morphologies in the three systems are

Table I. Scattering Vector and Long Periodicity (L) of PP–EP/EVAx/Organoclay Nanocomposites

Sample	q_{max1} (1/nm)	L_1 (nm)	q_{max2} (1/nm)	L_2 (nm)
Cloisite 20A	2.51	2.50	5.19	1.21
PP-EP/EVA9/C20A	1.78	3.52	3.69	1.70
PP-EP/EVA18/C20A	1.56	4.01	3.12	2.01
PP-EP/EVA28/C20A	1.49	4.20	3.00	2.09

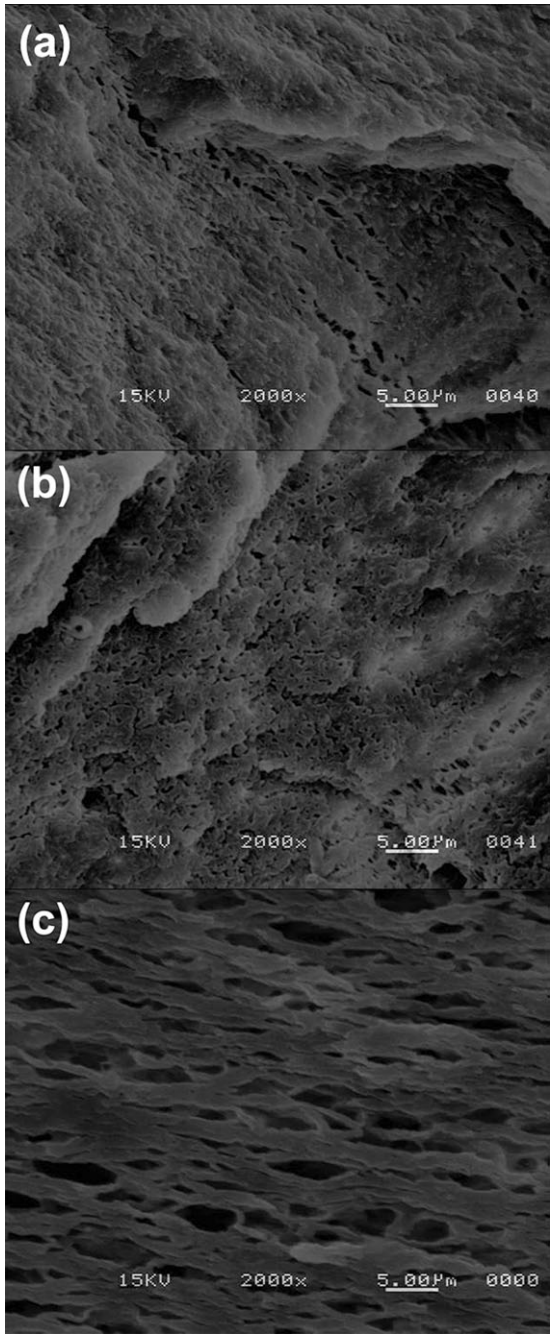

Figure 4. SEM images of PP–EP/EVA/organoclay nanocomposites: (a) PP–EP/EVA9/C20A, (b) PP–EP/EVA18/C20A, and (c) PP–EP/EVA28/C20A.

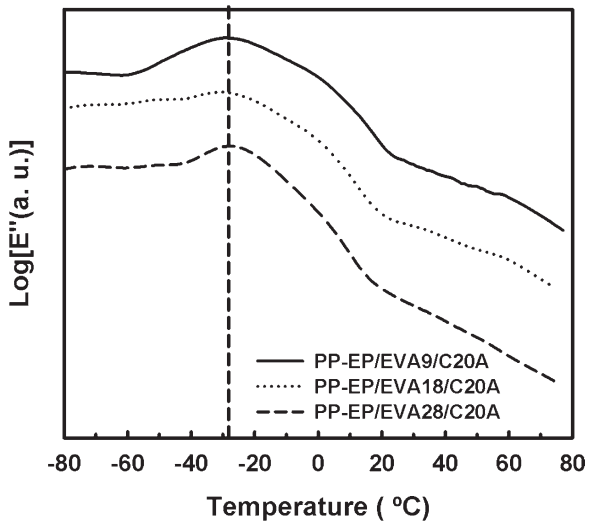

Figure 5. Loss modulus as a function of temperature of PP–EP/EVAx/C20A nanocomposites with different VA content.

consistent with the previously reported morphologies in the PP–EP/EVA compatibility range. At low-VA contents [Figure 4(a)], small spherical domains are found, with an average 0.5 μm in diameter. At high-VA contents [Figure 4(c)], larger elongated EVA domains with an average 5 μm length are observed.

To prove if VA content influences on compatibility of PP–EP/EVAx phases, DMA storage modulus (E'') analysis were obtained. In Figure 5, it is shown the region corresponding to the glass transition (T_g) of the nanocomposites where a single signal is observed. In previous studies of PP–EP/EVA blends, it was found that displacements in T_g are associated to changes in the compatibility.[24] In this case, none important changes in the T_g values of three nanocomposite systems were found, independently of VA content in EVA, which suggests that there are not differences in compatibility.

Thermal Stability

Some authors[26–28] have reported that organoclay commonly enhances thermal stability of polymers. Therefore, we examined the temperature dependence of the weight loss characteristic of PP–EP/EVAx blends and PP–EP/EVAx/C20A nanocomposites as a function of VA content. Thermograms in Figure 6 indicate that all samples consist of two-step decompositions. It has been reported by different authors that EVAs exhibit this behavior.[22,29,30] The first decomposition step is linked to the loss of acetic acid of EVA from 300 to 380°C as well as the decomposition of the organomodifier of nanoclay (Figure 6). The second one corresponds to the loss of transvinylenes formed and accompanied by the main-chain scission. Also, the second weight-loss decomposition is related to PP–EP degradation. In this case, thermal stability of blends and nanocomposites depends on VA content. For both PP–EP/EVA9 and PP–EP/EVA9/C20A, the weight loss is less evident than the other two cases (18 and 28 wt % VA) due to the lower VA content (see also Table II). It is observed that PP–EP/EVAx/C20A nanocomposites have better thermal stability than PP–EP/EVAx blends

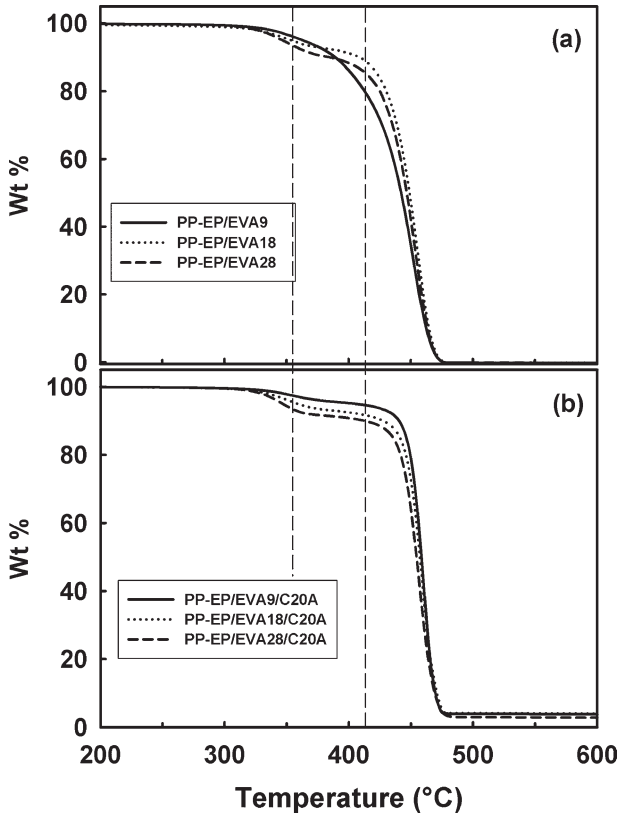

Figure 6. TGA curves of (a) PP–EP/EVA blends with different VA content and (b) PP–EP/EVA/organoclay nanocomposites.

mainly because of nanoclay platelets that may act as barriers for heat diffusion.[31,32]

Considering that intercalated–exfoliated nanoclay is preferentially confined within the EVA phase, then, as the EVA starts to degrade, the deacetylation processes and the decomposition of the organomodifier makes the silicate layers less organophilic and the polymer less polar, that is, less compatible with the silicate layers.[33] These phenomena lead to a collapse of the clay platelets. However, collapsed platelets contribute to the retardation of the thermal-degradation process due to the decrease in heat diffusion.

Table II. Maximum Temperatures at the Main Degradation Peaks and Weight Loss (%) of PP–EP/EVAx Mixtures and Their Nanocomposites With Different VA Content: 9, 18, and 28 wt %

Sample	*T* peak 1 (°C)	Weight loss (wt %)	*T* peak 2 (°C)	Weight loss (wt %)
PP-EP/EVA9	353.6	6.05	453.0	94.20
PP-EP/EVA9/C20A	357.4	4.48	459.2	91.64
PP-EP/EVA18	351.4	7.44	453.4	92.74
PP-EP/EVA18/C20A	353.3	7.03	458.2	88.88
PP-EP/EVA28	347.2	9.79	452.9	90.44
PP-EP/EVA28/C20A	351.1	8.62	456.1	88.50

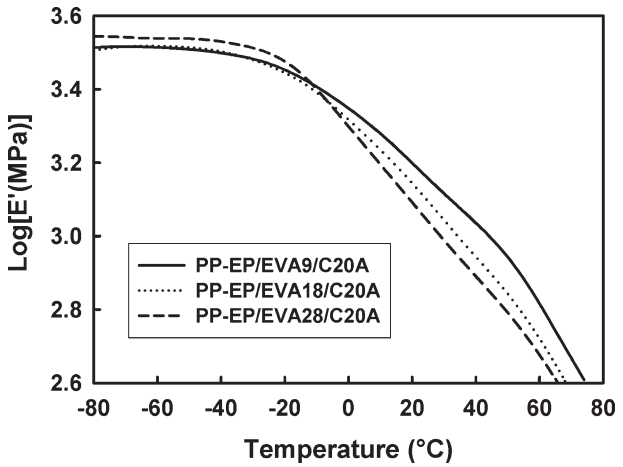

Figure 7. Storage modulus as a function of temperature of PP–EP/EVAx/C20A nanocomposites with different VA content.

Comparing the curves of second weight loss of nanocomposites in Figure 6, it is observed that PP–EP/EVA9/C20A shows better thermal stability than PP–EP/EVA18/C20A and PP–EP/EVA28/C20A. Slight differences between thermal stability of blends and nanocomposites may be attributed to the major formation of unsaturated poly(ethylene-*co*-acetylene), which show chain scission at allylic position, after the loss of acetic acid in EVA28 as reported by Costache et al.[34] In general, these results suggest that nanoclays slightly retard the degradation process (in particular of the second step), as better shown in Table II. Thermal retardation due to nanoclay must occur through a mechanism that involves low-thermal conductivity of the nanoclay layers, together with their gas impenetrability, inhibiting as a consequence molecular mobility of the low-molecular weight by-products during degradation.[35]

The dynamic mechanical properties of nanocomposites were studied through the storage modulus, and the results presented in Figure 7 show two particular effects. At low temperatures (from −80 to −20°C), it is observed that high-VA content promotes small increases in storage modulus (E'), that is, higher rigidity. Below −20°C, that is, below the polymeric components T_g, the small differences in storage modulus could only be attributed to the higher level of intercalation–exfoliation as the VA contents increase. In this case, it is associated with the major presence of nanoclay population I as observed in micrography c of Figure 3. At high temperatures (from −20 to 80°C), that is, above T_g, modulus decreases for all cases. At this higher temperature range, the elastomeric behavior of polymeric materials predominates over the polymer–organoclay interaction showed by PP–EP/EVA9/C20A nanocomposite that possesses the higher value in storage modulus (E').

CONCLUSIONS

At least two nanoclay populations with different periodicities were present in PP–EP/EVAx/organoclay nanocomposites. EVA copolymer plays an important role in the system, promoting the intercalation of the nanoclay platelets depending on the VA content. The better intercalation–exfoliation effect was assigned to the higher amount of polar groups of EVA in PP–EP/EVA28/C20A nanocomposite; resulting the strong noncovalent interactions of VA groups and the charged regions in the clay surface. There were two morphologies in EVA domains that agree with the previously reported in the compatibility range of PP–EP/EVA blends. Low-VA contents generated small spherical domains, and high-VA contents rendered elongated domains. From loss modulus results, it was found that there were not differences in compatibility of nanocomposites, because the T_g's did not change. Organoclay slightly retards thermal degradation of heterophasic nanocomposites due to nanoclay, and its collapsed platelets act as a barrier for heat diffusion. At low temperature, below T_g, higher storage modulus was obtained for higher VA (EVA28) content nanocomposites, and this was attributed to the slightly higher level of intercalation–exfoliation. At higher temperatures, above T_g, modulus decreases for all cases, but PP–EP/EVA28/C20A decreases in greater extent probably due to the predominance of the elastomeric behavior of polymeric materials over polymer–organoclay interaction.

ACKNOWLEDGMENTS

The authors thank the Mexican National Council for Science and Technology (CONACYT) for its financial support to carry out this study through project SEP-2005-P49143-Y (24606) and SEP-CONACyT 50177. The authors also thank R. Cedillo G., B. Huerta M., P. Siller F., M. Palacios M., J. Rodríguez V, J. Zamora R., M. Lozano E., F. Chavez, F. Zendejo, and J. Lopez for their experimental measurements and some suggestions.

REFERENCES

1. Alexandre, M.; Dubois, P. *Mater. Sci. Eng. R* **2000**, *28*, 1.
2. Giannelis, E. P. *Adv. Mater.* **1996**, *8*, 29.
3. Shah, R. K.; Hunter, D. L.; Paul, D. R. *Polymer* **2005**, *46*, 2646.
4. Choi, M. H.; Chung, I. J.; Lee, J. D. *Chem. Mater.* **2000**, *12*, 2977.
5. Kato, M.; Usuki, A.; Okada, A. *J. Appl. Polym. Sci.* **1997**, *66*, 1781.
6. Liu, L.; Qi, Z.; Zhu, X. *J. Appl. Polym. Sci.* **1999**, *71*, 1133.
7. Vaia, R. A.; Giannelis, E. P. *Macromolecules* **1997**, *30*, 8000.
8. Zanetti, M.; Lomakin, S.; Camino, G. *Macromol. Mater. Eng.* **2000**, *279*, 1.
9. Fornes, T. D.; Yoon, P. J.; Hunter, D. L.; Keskkula, H.; Paul, D. R. *Polymer* **2002**, *43*, 5915.
10. Yoon, P. J.; Hunter, D. L.; Paul, D. R. *Polymer* **2003**, *44*, 5323.
11. Hasegawa, N.; Kawasumi, M.; Kato, M.; Usuki, A.; Okada, A. *J. Appl. Polym. Sci.* **1998**, *67*, 87.
12. Hotta, S.; Paul, D. R. *Polymer* **2004**, *45*, 7639.
13. Wang, K. H.; Choi, M. H.; Koo, C. M.; Choi, Y. S.; Chung, I. *J. Polymer* **2001**, *42*, 9819.
14. Alexandre, M.; Beyer, G.; Henrist, C.; Cloots, R.; Rulmont, A.; Jérôme, R.; Dubois, P. *Macromol. Rapid Commun.* **2001**, *22*, 643.

15. Zhong, Y.; De Kee, D. *Polym. Eng. Sci.* **2005**, *45*, 469.
16. Pasanovic-Zujo, V.; Gupta, R.; Bhattacharya, S. *Rheol. Acta* **2004**, *43*, 99.
17. Valera-Zaragoza, M.; Ramírez-Vargas, E.; Medellín-Rodríguez, F. J.; Huerta-Martínez, B. M. *Polym. Degrad. Stab.* **2006**, *91*, 1319.
18. Valera-Zaragoza, M.; Ramírez-Vargas, E.; Medellín-Rodríguez, F. J. *J. Appl. Polym. Sci.* **2008**, 108 1986.
19. Hong, C. H.; Lee, Y. B.; Bae, J. W.; Jho, J. Y.; Nam, B. U.; Hwang, T. W. *J. Appl. Polym. Sci.* **2005**, *98*, 427.
20. La Mantia, F. P.; Lo Verso, S.; Dintcheva, N. T. *Macromol. Mater. Eng.* **2002**, *287*, 909.
21. Dumont, M. J.; Reyna-Valencia, A.; Emond, J. P.; Bousmina, M. *J. Appl. Polym. Sci.* **2007**, *103*, 618.
22. Zhang, W. A.; Chen, D.; Zhao, Q.; Fang, Y. E. *Polymer* **2003**, *44*, 7953.
23. Medellin-Rodríguez, F. J.; Hsiao, B. S.; Chu, B.; Fu, B. X. *J. Macromol. Sci. B* **2003**, *42*, 201.
24. Ramírez-Vargas, E.; Medellín-Rodríguez, F. J.; Navarro-Rodríguez, D.; Avila-Orta, C. A.; Solís-Rosales, S. G.; Lin, J. S. *Polym. Eng. Sci.* **2002**, *42*, 1350.
25. Huerta-Martínez, B. M.; Ramírez-Vargas, E.; Medellín-Rodríguez, F. J.; García, R. C. *Eur. Polym. J.* **2005**, *41*, 519.
26. Gilman, J. W. *Appl. Clay Sci.* **1999**, *15*, 31.
27. Ratnayake, U. N.; Haworth, B.; Hourston, D. J. *J. Appl. Polym. Sci.* **2009**, *112*, 320.
28. Zhu, J.; Wilkie, C. A. *Polym. Int.* **2000**, *49*, 1158.
29. Dutta, S. K.; Bhowmick, A. K.; Mukunda, P. G.; Chaki, T. K. *Polym. Degrad. Stab.* **1995**, *50*, 75.
30. Zanetti, M.; Camino, G.; Thomann, R.; Mülhaupt, R. *Polymer* **2001**, *42*, 4501.
31. Zanetti, M.; Costa, L. *Polymer* **2004**, *45*, 4367.
32. Yano, K.; Usuki, A.; Okada, A.; Kurauchi, T.; Kamigaito, O. *J. Polym. Sci., Part A: Polym. Chem.* **1993**, *31*, 2493.
33. Pastore, H. O.; Frache, A.; Boccaleri, E.; Marchese, L.; Camino, G. *Macromol. Mater. Eng.* **2004**, *289*, 783.
34. Costache, M. C.; Jiang, D. D.; Wilkie, C. A. *Polymer* **2005**, *46*, 6947.
35. Pramanik, M.; Srivastava, S.; Samantaray, B.; Bhowmick, A. *Macromol. Res.* **2003**, *11*, 260.